

# Improved Quality Control for QuikSCAT Near Real-time Data

S. Mark Leidner\*, Ross N. Hoffman, and Mark C. Cerniglia

Atmospheric and Environmental Research Inc., Lexington, Massachusetts

## Abstract

SeaWinds on QuikSCAT, launched in June 1999, provides a new source of surface wind information over the world's oceans. This new window on global surface vector winds has been a great aid to real-time operational users, especially in remote areas of the world. As with in situ observations, the quality of remotely-sensed geophysical data is closely tied to the characteristics of the instrument. But remotely-sensed scatterometer winds also have a whole range of additional quality control concerns different from those of in situ observation systems. The retrieval of geophysical information from the raw satellite measurements introduces uncertainties but also produces diagnostics about the reliability of the retrieved quantities. A working knowledge of the limitations of the instrument and its wind retrieval algorithms will improve the use of the near real-time QuikSCAT winds.

A characteristic swath of QuikSCAT data in the Western Atlantic illustrates typical benefits and deficiencies of these valuable data. The effects of the instrument's design and wind retrieval algorithm on the quality of the data under normal and extraordinary circumstances are presented. The effects of high and low winds, heavy rain, and aspects of the instrument's measurement geometry will be illustrated by selected cases from the swath.

## 1. Introduction

The primary mission of the SeaWinds instrument on the QuikSCAT satellite is to retrieve the surface vector wind over the global ocean (Shirtilffe 1999). SeaWinds wind vectors are generally of high quality, but error characteristics are complex. The two goals of this paper are to show how well the high quality, high resolution SeaWinds data depict the ocean surface wind field, and to provide some insight into the data

errors. We will illustrate the types of errors that occur due to rain contamination and ambiguity removal. We will also give examples of how the quality of the retrieved winds varies across the satellite track, and varies with wind speed.

SeaWinds is an active, Ku-band microwave radar operating near 14 *Ghz* and is sensitive to centimeter-scale or capillary waves on the ocean surface. These waves are usually in equilibrium with the wind. Each radar backscatter observation samples a patch of ocean about  $25 \times 35$  *km*. The vector wind is retrieved by combining several backscatter observations made from multiple viewing geometries as the scatterometer passes overhead. The resolution of the retrieved winds is  $\sim 25$  *km*.

Backscatter from capillary waves on the ocean surface, therefore, is the desired signal, since therein lies information about the vector wind. However, many other factors can influence backscatter observations and thereby effect the retrieved winds. Rain, for example, changes the ocean surface roughness, as well as attenuating and scattering the radar energy (Jones et al. 2000b; Mears et al. 2000). Light winds are also troublesome, since the ocean surface acts more like a reflecting mirror than a scatterer. Also, the measurement geometry of SeaWinds results in error characteristics which vary across the satellite swath.

Given these and other caveats about the data, we use a single swath of data over the North Atlantic to illustrate the benefits and potential pitfalls of vector winds from SeaWinds (§ 3, § 4 and § 5). The illustrations presented should improve everyday use of the data, both qualitative and quantitative, through a deepened understanding of the instrument, its principles of operation and retrieval of vector winds. In this paper, we use only the near real-time (NRT) SeaWinds data produced by NOAA/NESDIS and distributed to operational users in BUFR format, since this is the data used at operational centers. A different science data product (SDP) is created by JPL and distributed by PO.DAAC in delayed mode in HDF format. Most published work makes use of the SDP. The important differences between the two

\* Corresponding author address: S. Mark Leidner, Atmospheric and Environmental Research, Inc., 131 Hartwell Avenue, Lexington, Massachusetts 02421; email [leidner@aer.com](mailto:leidner@aer.com)

data sets are listed in § 2. We conclude with a short review of the current and potential uses of SeaWinds data (§ 6).

## 2. The SeaWinds instrument

### a. Timeline

The NASA SeaWinds space-borne microwave radar on QuikSCAT was launched 7:15 p.m. Pacific Daylight Time 19 June 1999 by a U.S. Air Force Titan II launch vehicle from Vandenberg AFB. SeaWinds was turned on 7 July and QuikSCAT achieved its operational inclined polar orbit, 803 km above the earth 10 July. Each orbit is  $\sim 100$  minutes long and the spacecraft travels at  $\sim 7$  km/s. There are about 15 orbits or “revs” (short for revolutions) per day or about 100 per week, and equatorial crossing points are separated by 2800 km. Every 57 orbits is a repeat. The orbital plane is perpendicular to the sunlight—local time at the ascending node is within 30 minutes of 600 am. The spacecraft is rarely in the earth’s shadow. (Note that QuikSCAT orbits start at the ascending equator crossing and QuikSCAT revs start closest to the South Pole.) The first scientifically valid QSCAT winds were acquired from rev 430 at 1839 UTC on 19 July 1999.

Since its launch, the SeaWinds instrument has produced ocean surface wind vectors reliably. The SeaWinds swaths cover over 90% of the earth’s surface in 24 hours. Anomalies tend to occur on holidays and weekends. There was a gyroscope failure on 1 January 2000. The instrument has gone into safe mode close to 4 July 2001 and 2002 probably due to cosmic rays over the South Atlantic Anomaly. On 11 May 2001 there was a GPS failure. In all cases the QuikSCAT team responded rapidly and effectively to restart the science data stream.

### b. Principles of operation

SeaWinds is the first scatterometer using a rotating antenna to be flown in space. Microwaves are transmitted to the surface in two pencil beams. Then, SeaWinds measures the backscatter from the earth’s surface at the satellite (Spencer et al. 2000). The fundamental measured quantity is,  $\sigma^0$ , or normalized radar cross-section. As the instrument’s 1-meter dish rotates at 18 rpm, two pencil beams oversample an 1800 km wide swath on the earth’s surface with both forward- and aft-looking

measurements. Forward and aft refer to beam footprints forward and aft of the spacecraft. Thus the backscatter values at a single location are observed within a time span of up to 290 seconds, increasing as the location approaches nadir. There are four types of measurements or “flavors”—inner-forward, outer-forward, inner-aft, and outer-aft. The SeaWinds NRT data contain one composite value for each flavor for each WVC. Here inner and outer refer to the inner and outer scan beams with look angles of  $39.876^\circ$  and  $45.890^\circ$  resulting in approximately constant incidence angles at the earth’s surface of  $45^\circ$  and  $53.6^\circ$ , respectively. Inner and outer are horizontally and vertically polarized, respectively. This diversity of measurements improves the ability of SeaWinds to determine wind direction. Note that in the far-swath there are only outer beam footprints, and thus only two flavors of  $\sigma^0$ . SeaWinds NRT processing requires at least one forward beam measurement and at least one aft beam measurement.

Since there are nominally four flavors of  $\sigma^0$  values in the center of the swath, but only two in the far-swath, wind retrievals in the far-swath are expected to be of lower quality. Further, we may identify two zones within the inner-swath, which we call the mid-swath and nadir-swath, of greater and lesser quality, respectively. The mid-swath ( $\sim 200 - 500$  km on either side of the satellite track) has the greatest diversity of azimuth and incidence angles, and hence the best quality data. The mid-swath is aka the “sweet spot”.

### c. Retrieval of geophysical quantities

The SeaWinds data are organized in a swath-based format, with 76 cross track cells. Since the cells are used to group  $\sigma^0$  data for wind vector retrieval they are called wind vector cells or WVCs. Unlike NSCAT, there is no “nadir” gap for SeaWinds. The nominal instrument measurement swath extends 900 km to either side of the nadir track. Thus, 72 WVCs, with 36 on either side of nadir, should accommodate nearly every  $\sigma^0$  measurement. Variations in spacecraft attitude and the local curvature of the earth will cause very few  $\sigma^0$  measurements to fall outside of the nominal measurement swath. To accommodate these measurements, the SeaWinds data products include 4 additional WVCs per row, two on either side of the measurement swath, for a total of 76 WVCs. For each across swath position or cell, there are 1624 rows of WVCs, from the beginning to the end of each

rev. Thus each WVC in the entire QuikSCAT mission may be uniquely identified by rev, row, and cell number.

The term “wind retrieval” encompasses the process of inverting the geophysical model function (e.g., Freilich and Dunbar 1993; Wentz and Smith 1999) for a given set of  $\sigma^0$  values to obtain (multiple) maximum likelihood estimates of the wind speed and direction. The inversion process is performed in a point-wise fashion (assuming each wind vector cell to be independent of its neighbors), and yields multiple solutions (ambiguities) due to the azimuthal variation of the model function. The process of ambiguity removal is performed in a field-wise fashion; the baseline algorithm used by SeaWinds is a vector median filter (Shaffer et al. 1991).

In scatterometry, the wind vector  $\mathbf{V}$  and backscatter coefficient or  $\sigma^0$  are related the geophysical model function,  $F$ .

$$\sigma^0 = F(\mathbf{V}; \alpha, \theta, f, p). \quad (1)$$

Here  $\alpha$  is the azimuth angle and  $\theta$  is the incidence angle of the observation,  $f$  is the frequency (13.4 GHz for SeaWinds), and  $p$  is the polarization. The geophysical model function developed for NSCAT (Wentz and Smith 1999) has been adjusted for SeaWinds (Perry 2001). This relationship neglects the effects of other surface parameters including sea surface temperature, surface salinity, surface contaminants, and swell (Brown 1983; Quilfen et al. 2001). Note that  $\mathbf{V}$  in (1) is the neutral stability wind at 10 m, and winds retrieved using this relationship will differ from the actual winds due to stability effects (Hoffman and Louis 1990). Also  $\mathbf{V}$  is relative to any ocean currents (Cornillon and Park 2001; Quilfen et al. 2001; Kelly et al. 2001).

Colocation studies show that if the ambiguity is properly resolved, scatterometer data are very accurate (Bourassa et al. 1997; Stoffelen 1998; Atlas et al. 1999; Freilich and Dunbar 1999; Wentz and Smith 1999). Colocation studies for QuikSCAT suggest comparable accuracy to NSCAT (Biber and Emery 2000; Bourassa et al. 2002).

This paper describes the attributes of the NRT SeaWinds data. These data are produced at NOAA/NESDIS with a 3 hours latency goal. This is a very stringent goal and almost all data are available within 3.5 hours. A NOAA/NESDIS web site (<http://manati.wvb.noaa.gov/quikscat/>) has displayed the QuikSCAT NRT winds since the general release of QuikSCAT data on 31 January 2000 by

JPL. The NRT SeaWinds BUFR data (Leidner et al. 1999) were first distributed to the operational community 23 February 2000. Rainflags were added to the BUFR data in mid-June 2000. Hurricane forecasters began using QuikSCAT data for the 2000-2001 hurricane season to aid detection of new tropical cyclones (Sharp et al. 2002). NRT SeaWinds data have been assimilated by the global analyses at NCEP since 1200 UTC 15 January 2002, and at ECMWF since 1800 UTC 21 January 2002.

The SeaWinds NRT processing algorithms are identical to the science data algorithms (Dunbar et al. 1995) except that the SeaWinds NRT data processing algorithms combine the finest grained  $\sigma^0$  measurements into fewer composites than the science data algorithms. This is necessary for the wind vector retrieval to meet operational latency requirements. In addition the NRT SeaWinds use NCEP forecasts to initialize the ambiguity removal, while the SDP processing uses NCEP analyses. The forecasts used are the so-called “aviation” forecasts and are generally no more than 12 hours old.

### 3. A representative swath of SeaWinds data

To illustrate features and uses of the data, we chose an interesting swath of data over the North Atlantic. All of our examples are taken from this single swath of data collected from 2200 through 2215 UTC 28 September 2000, during the descending pass of QuikSCAT rev 6659. Fig. 1 shows the selected wind vectors (thinned, for clarity, to every fourth wind vector cell along- and across-track) overlaid on a GOES satellite infrared image valid 2215 UTC 28 September 2000. Winds suspected of contamination by rain are highlighted in blue. NCEP mean sea-level pressure analysis valid at 0000 UTC 29 September is also plotted to corroborate features in the satellite data. This swath includes Hurricane Isaac near its peak intensity. The swath also includes large-scale trough north of Isaac between two synoptic centers of high pressure. As described in § 2, SeaWinds has no missing data near nadir and synoptic-scale features may be observed in the surface wind fields. Easterly winds are evident in the tropics in the scatterometer winds. Further to the north, scatterometer winds show anticyclonic flow around the two high pressure systems west and east of the low pres-

sure trough. Surface winds in the cloudy trough of low pressure are somewhat chaotic between the two centers of high pressure (to the northwest and southeast). The GOES satellite image shows embedded regions of convection in the low pressure trough. As seen in the NCEP MSLP analysis, there are two lobes of low pressure within the trough. There is rain contamination of a number of wind vectors in this region and their effect on the use of the data will be shown in § 4. The evidence of rain contamination in wind retrievals will be presented in § 5.

#### 4. An analysis impact example of SeaWinds data

Here we show an example of the impact of SeaWinds data on the analysis of ocean surface winds. We use a variational data assimilation method for two-dimensional wind fields, 2d-VAR. As in all variational assimilation schemes, 2d-VAR combines observations and an *a priori* or first guess estimate of the solution. The analysis is found through a minimization procedure which balances the best fit to observations with meteorological constraints on the solution. For a full description of the technique and applications of 2d-VAR see Hoffman et al. (2002) and Henderson et al. (2002).

The 2d-VAR analysis region is the area depicted in Fig. 1. The analysis grid is a  $1^\circ \times 1^\circ$  latitude/longitude grid (*i.e.*, no map projection). A three-hour forecast from NCEP's aviation forecast model provides the background wind field and is valid at 2100 UTC 28 September. We chose a short-term forecast closest in time to the scatterometer observations for the background, since this is the practice at many operational centers. SeaWinds data from rev 6659 (see Fig. 1) are used in the analysis. The results of two analyses are presented here: ALLOBS uses all available observations in the region (12004), while NORAIN uses only those observations free from rain contamination (10754). Both experiments use two winds solutions at each data point, and 2d-VAR chooses one during the analysis. For more information on QC methods for pairs of scatterometer winds see Hoffman et al. (2002).

The overall impact of 2d-VAR may be seen by comparing the observations to the background and then to the analysis. In the mean, the scatterometer winds are  $0.41 \text{ m s}^{-1}$  higher than the NCEP background

winds with a standard deviation of  $1.8 \text{ m s}^{-1}$ . In the analysis, the scatterometer winds are only  $0.17 \text{ m s}^{-1}$  higher with a standard deviation of  $1.3 \text{ m s}^{-1}$ . Therefore, 2d-VAR has created a surface wind analysis which fits the scatterometer data better in both mean and rms wind speed. (It should be noted that scatterometer winds are generally higher than winds from global forecast models because of the difference in scales represented; scatterometer:  $25 \text{ km}$ , global forecast model:  $100 - 200 \text{ km}$ ). A similar result is found for the ALLOBS analysis, but rain contamination increases both the mean and rms differences for comparisons with both background and analysis (see Table 1).

Scatterometers have the ability to detect mesoscale features which may not be present in large-scale analyses. Fig. 2 depicts just such a case. SeaWinds detected a small circulation embedded in the southern lobe of low pressure in the synoptic trough. Fig. 2 upper left panel shows the NCEP background wind field in the vicinity of the trough. The NCEP 3-hr forecast has simple shearing flow along the front. Fig. 2 upper right panel shows the 2d-VAR NORAIN analysis. A closed circulation is found along the front, which is suggested by the NCEP MSLP analysis (Fig. 2 lower right) and supported by a time series of succeeding MSLP analyses (not shown). The ALLOBS analysis is very poor since rain-contaminated data are used (Fig. 2 lower left). The speed and direction of the winds in these areas of heavy rain make them unsuitable for use in data assimilation.

#### 5. Factors influencing SeaWinds data quality

Careful quality control is vital to consistently obtain high quality results. Understanding of the instrument and algorithm characteristics provides insights into the factors controlling data quality for SeaWinds. In § 2 we briefly described the viewing geometry, the effect of rain, and the accuracy of SeaWinds winds. In this section we reprise each of these in more detail with regard to potential effects on data quality. We present typical examples of data and discuss the associated data quality concerns, for different parts of the swath, for different wind speeds, and for rain versus no rain. The loss function for representative WVCs presented here graphically illustrate the work-

ings of the wind retrieval algorithm.

*a. Scatterometer objective functions and wind retrieval*

Many of the special data characteristics of a scatterometer are revealed by examining the likelihood function which is maximized during the wind retrieval. In SeaWinds processing, various approximations make the process of maximizing the likelihood equivalent to minimizing an objective function which is equal to the sum of squared scaled differences between observed and simulated backscatter. Each difference is scaled by its expected error. The loss function is precisely defined in the appendix.

The nature of the ambiguity of scatterometer data is apparent when the function is plotted with respect to the retrieved values of the  $u$  and  $v$  wind components. Because the objective function has such a large range, for plotting purposes we add 4 to the objective function, set values above 400 equal to 400, and convert to decibels. In the plots the values run from 6 *dB* (red) to 26 *dB* (blue), and we superimpose the first five 1 *dB* contours to the plot (the maximum value contoured is 12 *dB*).

A typical example for QuikSCAT is shown in the bottom panel of Fig. 3. But first consider the top panel showing the result of using just one backscatter measurement, in this case the forward outer beam. Every point on the green dotted curve is a wind which exactly fits the single observation. The single backscatter observation does not tell us anything about wind direction, but does strongly indicate a minimum plausible wind speed of  $\sim 4.5$  *m/s*. In other words, the backscatter measurement implies a lower limit of surface roughness. Even if the viewing geometry maximizes the apparent roughness, the wind must be  $\geq 4.5$  *m/s*. On the other hand wind speeds  $> 15$  *m/s* are unlikely. The modulation of wind speed with wind direction shown by the green curve makes it impossible to deduce an accurate wind speed from the single measurement, but it is this modulation which makes wind vector retrieval possible from multiple measurements.

This is seen in the middle panel of Fig. 3 which shows the result of using both forward and aft outer beam measurements. This scenario is similar to the nominal mode for the original Seasat satellite scatterometer. The green dotted curve is as before. Points on the black dotted curve exactly fit the aft outer beam observation. Now there are four distinct

minima, at the intersections of these two curves, corresponding to four wind ambiguities, plotted here as arrows. In this case, the ambiguities are all perfectly consistent with both measurements. Therefore without additional information, all four are considered to be equally likely. As the wind, viewing geometry, and/or observational errors vary, the two quasi-ellipses may change orientation and aspect ratio leading to zero to four intersections or near intersections, and a corresponding number of retrieved wind ambiguities.

Finally the bottom panel, adds the inner beam measurements as well. Wind arrows plotted here are the operational NESDIS NRT retrievals. With the addition of the inner beam measurements, there is less symmetry than in the middle panel, and there are no intersections of all four quasi-ellipses. In the absence of errors—instrument noise, model function error, etc.—there would be one intersection. In the real data case we must take the minima of the objective function as “best” estimates of the wind. Note that it is now possible to rank the ambiguities by likelihood. The ambiguity with the greatest eastward component is most likely. However it is the ambiguity with the greatest northward component which is chosen by the ambiguity removal algorithm, and which is consistent with the synoptic situation. This cell is in a broad region of southerly winds (not shown).

*b. Swath-dependent characteristics*

The viewing geometry varies across the swath and with the wind direction, resulting in different ambiguity patterns. Some examples are shown in Fig. 4. The upper panel shows one complete row of selected wind vectors plotted on top of a GOES satellite image. The wind barbs alternate colors to help distinguish odd (black) and even (red) numbered cells. The lower three panels highlight the objective function at different points across the swath. Cell 38 shows behavior which may be seen close to nadir. In such cases, although 1, 2, 3 or 4 ambiguities may be defined, there is in fact little directional information and limited speed information. For cell 38, the wind speed is probably in the range 3 – 5.5 *m/s* and the wind direction is unlikely to be from the North, but one can say little more. The poor definition of wind direction near nadir is a consequence of having essentially only two azimuth angles. In these cases the quasi-ellipses are well aligned—if they were perfectly aligned, the pattern would reduce to that of a

single observation (top panel of Fig. 3). Cell 18 is a good example of the objective function in the “sweet spot” or near-optimal viewing geometry. Four ambiguities are found, and the minima are well-defined. Two minima are dominant and these two are approximately opposed. The direction of the selected ambiguity is easy to verify since the observation is in the environment of Isaac. For cell 4, two ambiguities are found and they are approximately opposed. At this point in the far swath, the minima, though clear, are more elongated than in the sweet spot because the diversity of azimuth viewing angles is quite small. This analysis of the QuikSCAT objective function suggests, and comparisons with other data sources show, an increase in the rms speed and directional error near nadir and at the far swath edges.

#### c. High and Low winds

Very high and very low winds are also problematic for the scatterometer. Since the GMF is tuned in part with buoy observations and gridded fields from weather forecast models, very small-scale, high winds are not present in these data sets. Consequently, winds above  $25 \text{ m s}^{-1}$  are not often retrieved, and when they are, the retrieved winds usually underestimate the true wind speed (e.g., Hurricane Isaac presented in § 3).

Low winds have very poor directional skill. Below a threshold wind speed no small waves are generated (Carswell et al. 1999), but the scatterometer footprint will usually average over a range of wind speeds (Plant 2000; Shankaranarayanan and Donelan 2001). Low directional skill is the consequence of a physical limitation of the instrument’s measurement principle. With no winds, the sea surface is like a smooth glass reflector, and there is virtually no backscatter.

Negative  $\sigma^0$  observations are indicative of very light winds. During processing an estimate of the noise is removed from the measurement. Therefore, for low wind speeds, when the true reflected power is very small, the estimated reflected power may be negative (Pierson 1989).

The  $\sigma^0$  measurements are stored in *dB* and cannot represent negative values. One bit of the  $\sigma^0$  quality flag, denoted *s* here, indicates whether the normal (ratio) space  $\sigma^0$  is negative. Thus

$$\sigma^0[\text{ratio}] = (-1)^s 10^{(\sigma^0[\text{dB}]/10)}.$$

Fig. 5 shows the objective function for a very low

winds case where two of the four  $\sigma^0$  values are negative. Notice that virtually no directional information is present.

#### d. Rain contamination

Rainflags have been developed for SeaWinds after the launch of QuikSCAT. Original plans paired SeaWinds with a passive microwave sensor that would have provided a rainflag. Instead a variety of alternative rainflags have been proposed, and several of these have been combined into a multi-dimensional histogram (MUDH) rain indicator and rainflag (Huddleston and Stiles 2000). The effect of rain on SeaWinds wind speed errors varies with the wind magnitude (Weissman et al. 2002). Thus Portabella and Stoffelen (2001) developed a quality control and rain detection procedure for SeaWinds that applies a wind speed dependent threshold to the normalized SeaWinds residual, *i.e.*, the degree of consistency of the observed backscatter and the retrieved wind. The Normalized Objective Function (NOF) developed by Mears et al. (2000) is based on a similar measure of consistency. Additional rainflags have been developed (Jones et al. 2000b; Boukabara et al. 2002) making use of brightness temperature inferred from the SeaWinds noise measurement (Jones et al. 2000a).

Fig. 6 shows an example of the kind of effect rain can have on SeaWinds observations. As in Fig. 4, the upper panel shows a highlighted row of selected wind vectors while the lower three panels show objective functions for selected cells. Cells 41 and 36 are rain free according to the MUDH and NOF rainflags, but cells 40-37 are affected by the heavy rain in the front. Notice that the minima in the rain-free cells are very much lower and better defined than in cell 39. Rain has equalized backscatter for cell 39 from all view points and virtually no wind direction signal remains. Also notice rain has nearly doubled the wind speed compared to neighboring rain-free cells.

## 6. Uses of SeaWinds data

SeaWinds and other scatterometer data in general have many potential uses.

SeaWinds and other scatterometer data help to detect and precisely locate TCs (Veldon et al. 2002; Ritchie et al. 2002) and extratropical cyclones. Pat-

terns in scatterometer winds make possible early detection of TCs and tropical depressions (Katsaros et al. 2001). The method of Sharp et al. (2002) detects TCs by calculating the vorticity on the SeaWinds WVC grid, and applying a threshold. Zierden et al. (2000) used NSCAT, the precursor to SeaWinds, to study cyclone surface pressure fields and frontogenesis, and Liu et al. (1997) used NSCAT to monitor the evolution of TCs. Scatterometer data can be used to specify the radius of gale force winds (Edson and Hawkins 2000; Hawkins and Helveston 1998), and in addition can depict the 2-D patterns of surface wind speed in storms.

SeaWinds and other scatterometer data are useful for weather analysis and forecasting (Atlas et al. 2001). These data have generally been shown to have a positive impact on Southern Hemisphere extratropics numerical weather prediction (NWP) and a neutral impact on Northern Hemisphere extratropics NWP (e.g., Andrews and Bell 1998), and a positive impact on NWP of tropical cyclones (e.g., Isaksen and Stoffelen 2000; Leidner et al. 2002).

SeaWinds and other scatterometer data improve our understanding of the physics of small scale ocean-atmosphere and atmosphere-topography interactions. Examples of such interactions include the South Georgia Island wind shadow (Freilich and Vanhoff 2003) and the Central American wind jets (Chelton et al. 2000a,b). Several investigators (Liu et al. 2000; Chelton et al. 2001; Polito et al. 2001) combined scatterometer data and satellite based SST analyses to discover a wave-like disturbance propagating in the ocean-atmosphere system near the equator. A similar phenomena was found to occur along the wake of a tropical cyclone (Lin et al. 2002).

SeaWinds and other scatterometers also provide fractional coverage of sea ice, monitor large ice bergs in all weather conditions, map different types of ice and snow, and detect the freeze/thaw line in tundra (Gohin et al. 1998; Ezraty and Cavanie 1999; Remund and Long 1999; Long et al. 2001; Drinkwater et al. 2002).

## 7. Acknowledgments

The authors thank their colleagues for many helpful discussions. We particularly thank Scott Dunbar (JPL) and Julia Figa Saldana (EUMETSAT). Data used in the research reported here were pro-

vided by the Jet Propulsion Laboratory (JPL) Physical Oceanography Distributed Active Archive Center (PO.DAAC), the National Centers for Environmental Prediction (NCEP), NESDIS, and the European Centre for Medium-Range Weather Forecasts (ECMWF). This research was supported by the SeaWinds NASA scatterometer project.

## 8. Appendix: Scatterometer loss function

The maximum likelihood estimator is the value of the objective function which is maximized, divided by the number of  $\sigma^0$  WVC-composites used. The objective function is the negative of the sum of squared differences between observed and modeled  $\sigma^0$  values, where each squared difference is normalized by its expected variance,  $\varepsilon^2$ . Three coefficients, denoted here as  $\alpha$ ,  $\beta$  and  $\gamma$ , are used to calculate  $\varepsilon^2$ , according to

$$\varepsilon^2 = [\alpha(1 + K_{pm}) - 1](\sigma^0)^2 + \beta\sigma^0 + \gamma.$$

Together the coefficients  $\alpha$ ,  $\beta$  and  $\gamma$  represent the effect of  $K_{pc}$ , the communication noise, and  $K_{pr}$ , the “radar equation” noise due to various geometrical and other instrument uncertainties. Also  $K_{pm}$  accounts for errors in the formulation of the model function. The value of  $\sigma^0$  used here should be the modeled value. That is, during wind retrieval, it is the estimate of  $\sigma^0$  based on the current estimate of the wind.

## References

- Andrews, P. L. and R. S. Bell, 1998: Optimizing the United Kingdom Meteorological Office data assimilation for ERS-1 scatterometer winds. *Mon. Wea. Rev.*, **126**, 736–746.
- Atlas, R., S. C. Bloom, R. N. Hoffman, E. Brin, J. Ardizzone, J. Terry, D. Bungato, and J. C. Jusem, 1999: Geophysical validation of NSCAT winds using atmospheric data and analyses. *J. Geophys. Res.*, **104**, 11405–11424.
- Atlas, R., R. N. Hoffman, S. M. Leidner, J. Sienkiewicz, T.-W. Yu, S. C. Bloom, E. Brin, J. Ardizzone, J. Terry, D. Bungato, and J. C. Jusem, 2001: The effects of marine winds

- from scatterometer data on weather analysis and forecasting. *Bull. Amer. Meteor. Soc.*, **82**, 1965–1990.
- Biber, S. and W. Emery, 2000: A comparison of QuikSCAT-1 wind vectors with in-situ measurements from buoys in the tropical Pacific and Atlantic. *Ocean Winds: Workshop on Present and Emerging Remote Sensing Methods*, P. Flament, ed., IFREMER, Brest, France, number 11 in CER-SAT News (Special Issue), scientific Topic No. 2.
- Boukabara, S.-A., R. N. Hoffman, C. Grassotti, and S. M. Leidner, 2002: Physically-based modeling of QSCAT SeaWinds passive microwave measurements for rain detection. *J. Geophys. Res.*, in press.
- Bourassa, M. A., M. H. Freilich, D. M. Legler, W. T. Liu, and J. J. O'Brien: 1997, Wind observations from new satellite and research vessels agree. *Trans. Amer. Geophys. Union*, **78**, 597–602.
- Bourassa, M. A., D. M. Legler, J. J. O'Brien, and S. R. Smith, 2002: SeaWinds validation with research vessels. *J. Geophys. Res.*, in press.
- Brown, R. A., 1983: On a satellite scatterometer as an anemometer. *J. Geophys. Res.*, **88**, 1663–1673.
- Carswell, J. R., W. J. Donnelly, R. McIntosh, M. A. Donelan, and D. C. Vandemark, 1999: Analysis of C and Ku-band ocean backscatter measurements under low-wind conditions. *J. Geophys. Res.*, **104**, 20687–20701.
- Chelton, D. B., S. K. Esbensen, M. G. Schlax, N. Thum, M. H. Freilich, F. J. Wentz, C. L. Gentemann, M. J. McPhaden, and P. S. Schopf, 2001: Observations of coupling between surface wind stress and sea surface temperature in the eastern tropical Pacific. *J. Climate*, **14**, 1479–1498.
- Chelton, D. B., M. H. Freilich, and S. K. Esbensen: 2000a, Satellite observations of the wind jets off the Pacific coast of Central America. Part I: Case studies and statistical characteristics. *Mon. Wea. Rev.*, **128**, 1993–2018.
- 2000b: Satellite observations of the wind jets off the Pacific coast of Central America. Part II: Regional relationships and dynamical considerations. *Mon. Wea. Rev.*, **128**, 2019–2043.
- Cornillon, P. and K.-A. Park, 2001: Warm core ring velocities inferred from NSCAT. *Geophys. Res. Lett.*, **28**, 575–578.
- Drinkwater, M., D. Long, and A. Bingham, 2002: Greenland snow accumulation estimates from scatterometer data. *J. Geophys. Res.*, in press.
- Dunbar, R. S. et al., 1995: Science algorithm specification for SeaWinds. Technical report, Jet Propulsion Laboratory, Pasadena, CA.
- Edson, R. T. and J. D. Hawkins, 2000: A comparison of scatterometer-derived wind data over tropical cyclones as determined from ERS-2 and QuikSCAT data. *24th Conference on Hurricanes and Tropical Meteorology*, American Meteorological Society, Boston, MA, 195–196.
- Ezraty, R. and A. Cavanie, 1999: Intercomparison of backscatter maps over Arctic sea ice from NSCAT and the ERS scatterometer. *J. Geophys. Res.*, **104**, 11471–11483.
- Freilich, M. H. and R. S. Dunbar, 1993: Derivation of satellite wind model functions using operational surface wind analyses: An altimeter example. *J. Geophys. Res.*, **98**, 14633–14649.
- 1999: The accuracy of the NSCAT 1 vector winds: Comparisons with National Data Buoy Center buoys. *J. Geophys. Res.*, **104**, 11231–11246.
- Freilich, M. H. and B. A. Vanhoff, 2003: The ocean surface wind field near South Georgia Island, Antarctica. *11th Conference on Interaction of the Sea and Atmosphere*, American Meteorological Society, Boston, MA, Long Beach, California.
- Gohin, F., A. Cavanie, and R. Ezraty, 1998: Evolution of the passive and active microwave signatures of a large sea ice feature during its  $2\frac{1}{2}$ -year drift through the Arctic Ocean. *J. Geophys. Res.*, **103**, 8177–8189.
- Hawkins, J. D. and M. J. Helveston, 1998: ERS-NSCAT capabilities/limitations in mapping tropical cyclone wind fields. *9th Conference on the Interaction of the Sea and Atmosphere*, American Meteorological Society, Boston, MA, 45–48.
- Henderson, J. M., R. N. Hoffman, S. M. Leidner, J. V. Ardizzone, R. Atlas, and E. Brin, 2002: A comparison of a two-dimensional variational analysis

- method and a median filter for NSCAT ambiguity removal. *J. Geophys. Res.*, accepted.
- Hoffman, R. N., S. M. Leidner, J. M. Henderson, R. Atlas, J. V. Ardizzone, and S. C. Bloom, 2002: A two-dimensional variational analysis method for NSCAT ambiguity removal: Methodology, sensitivity, and tuning. *J. Atmos. Ocean. Technol.*, accepted.
- Hoffman, R. N. and J.-F. Louis, 1990: The influence of atmospheric stratification on scatterometer winds. *J. Geophys. Res.*, **95**, 9723–9730.
- Huddleston, J. N. and B. W. Stiles, 2000: A multidimensional histogram rain-flagging technique for SeaWinds on QuikSCAT. *International Geoscience and Remote Sensing Symposium (IGARSS)*, IEEE, New York, Honolulu, Hawaii, 1232–1234.
- Isaksen, L. and A. Stoffelen, 2000: ERS scatterometer wind data impact on ECMWF's tropical cyclone forecasts. *IEEE Trans. Geosci. Remote Sens.*, **38**, 1885–1892.
- Jones, W. L., R. Mehershahi, J. Zec, and D. G. Long, 2000a, SeaWinds on QuikSCAT radiometric measurements and calibration. *International Geoscience and Remote Sensing Symposium (IGARSS)*, IEEE, New York, Honolulu, Hawaii, 1027–1029.
- Jones, W. L., M. Susanj, J. Zec, and J.-D. Park, 2000b, Validation of QuikSCAT radiometric estimates of rain rate. *International Geoscience and Remote Sensing Symposium (IGARSS)*, IEEE, New York, Honolulu, Hawaii, 1229–1231.
- Katsaros, K. B., E. B. Forde, P. Chang, and W. T. Liu, 2001: QuikSCAT's SeaWinds facilitates early identification of tropical depressions in 1999 hurricane season. *Geophys. Res. Lett.*, **28**, 1043–1046.
- Kelly, K. A., S. Dickinson, M. J. McPhaden, and G. C. Johnson, 2001: Ocean currents evident in satellite wind data. *Geophys. Res. Lett.*, **28**, 2469–2472.
- Leidner, S. M., R. N. Hoffman, and J. Augenbaum, 1999: *SeaWinds Scatterometer Real-Time BUFR Geophysical Data Product*. Atmospheric and Environmental Research, Inc., Cambridge, MA, 2.2.0 edition.
- Leidner, S. M., L. Isaksen, and R. N. Hoffman, 2002: Impact of NSCAT winds on tropical cyclones in the ECMWF 4D-Var assimilation system. *Mon. Wea. Rev.*, in press.
- Lin, I.-I., W. T. Liu, C.-C. Wu, J. C. Chiang, and C.-H. Sui, 2002: Space-based observations of modulation of boundary layer winds by typhoon-induced upper ocean cooling. *J. Geophys. Res.*, 2002GL015674R, in press.
- Liu, W. T., W. Tang, and R. S. Dunbar, 1997: Scatterometer observes extratropical transition of Pacific typhoons. *Trans. Amer. Geophys. Union*, 237+240.
- Liu, W. T., X. Xie, P. S. Polito, S. Xie, and H. Hashizume, 2000: Atmosphere manifestation of tropical instability waves observed by QuikSCAT and Tropical Rain Measuring Missions. *Geophys. Res. Lett.*, **27**, 2545–2548.
- Long, D. G., M. R. Drinkwater, B. Holt, S. Saatchi, and C. Bertoia, 2001: Global ice and land climate studies using scatterometer image data. *Trans. Amer. Geophys. Union*, **82**, 503.
- Mears, C., D. Smith, and F. Wentz, 2000: Detecting rain with QuikSCAT. *International Geoscience and Remote Sensing Symposium (IGARSS)*, IEEE, New York, Honolulu, Hawaii, 1235–1237.
- Perry, K. L., 2001: QuikSCAT science data product user's manual, overview and geophysical data products. Version 2.2, Jet Propulsion Laboratory, Pasadena, CA, [JPL D-18053].
- Pierson, W. J., Jr., 1989: Probabilities and statistics for backscatter estimates obtained by a scatterometer. *J. Geophys. Res.*, **94**, 9743–9759.
- Plant, W. J., 2000: Effects of wind variability on scatterometry at low wind speeds. *J. Geophys. Res.*, **105**, 16899–16910.
- Polito, P., J. P. Ryan, W. T. Liu, and F. P. Chavez, 2001: Oceanic and atmospheric anomalies of tropical instability waves. *Geophys. Res. Lett.*, **28**, 2233–2236.
- Portabella, M. and A. Stoffelen, 2001: On quality control and rain detection of SeaWinds. *J. Atmos. Ocean. Technol.*, **18**, 1171–1183.

- Quilfen, Y., B. Chapron, and D. Vandemark, 2001: The ERS scatterometer wind measurement accuracy: Evidence of seasonal and regional biases. *J. Atmos. Ocean. Technol.*, **18**, 1684–1697.
- Remund, Q. P. and D. G. Long, 1999: Sea ice extent mapping using Ku band scatterometer data. *J. Geophys. Res.*, **104**, 11515–11527.
- Ritchie, E., J. Simpson, W. T. Liu, C. Veldon, K. Brueske, and J. Halvorsen: 2002, A closer look at hurricane formation and intensification using new technology. *Coping with Hurricanes*, R. Simpson, M. Garstang, and R. Anthes, eds., American Geophysical Society, American Geophysical Society, Washington, DC, chapter 12.
- Shaffer, S. J., R. S. Dunbar, S. V. Hsiao, and D. G. Long, 1991: A median-filter-based ambiguity removal algorithm for NSCAT. *IEEE Trans. Geosci. Remote Sens.*, **29**, 167–174.
- Shankaranarayanan, K. and M. A. Donelan, 2001: A probabilistic approach to scatterometer model function verification. *J. Geophys. Res.*, **106**, 19969–19990.
- Sharp, R. J., M. A. Bourassa, and J. J. O'Brien, 2002: Early detection of tropical cyclones using SeaWinds-derived vorticity. *Bull. Amer. Meteor. Soc.*, **83**, 879–889.
- Shirtiliffe, G. M., 1999: QuikSCAT science data product user's manual, overview and geophysical data products. Version 1.0, Jet Propulsion Laboratory, Pasadena, CA, [JPL D-18053].
- Spencer, M. W., C. Wu, and D. G. Long, 2000: Improved resolution backscatter measurements with the SeaWinds pencil-beam scatterometer. *IEEE Trans. Geosci. Remote Sens.*, **38**, 89–104.
- Stoffelen, A., 1998: Toward the true near-surface wind speed: Error modeling and calibration using triple collocation. *J. Geophys. Res.*, **103**, 7755–7766.
- Veldon, C., K. Bruske, C. Kummerow, W. T. Liu, J. Simpson, S. Braun, and R. Anthes, 2002: The burgeoning role of weather satellites. *Coping with Hurricanes*, R. Simpson, M. Garstang, and R. Anthes, eds., American Geophysical Society, American Geophysical Society, Washington, DC, chapter 11.
- Weissman, D. E., M. A. Bourassa, and J. Tongue, 2002: Effects of rain rate and wind magnitude on SeaWinds scatterometer wind speed errors. *J. Atmos. Ocean. Technol.*, **19**, 738–746.
- Wentz, F. J. and D. K. Smith, 1999: A model function for the ocean-normalized radar cross section at 14 GHz derived from NSCAT observations. *J. Geophys. Res.*, **104**, 11499–11514.
- Zierden, D. F., M. A. Bourassa, and J. J. O'Brien, 2000: Cyclone surface pressure fields and frontogenesis from NASA Scatterometer (NSCAT). *J. Geophys. Res.*, **105**, 23967–23981.

---

**Table 1:** *Mean and standard deviation of differences between the background wind field and observations, and the analyzed wind field and observations.*

<b>Differences</b>	<i>N</i>	<i>mean</i>	<i>std.dev.</i>
<b>NCEP background-ALLOBS</b>	12004	-0.846	2.571
<b>NCEP background-NORAIN</b>	10754	-0.412	1.833
<b>ALLOBS analysis-ALLOBS</b>	12004	-0.288	2.037
<b>NORAIN analysis-NORAIN</b>	10754	-0.179	1.279

**Fig. 1:** GOES satellite infrared image valid 2215 UTC 28 September 2000 over the Western Atlantic with part of QuikSCAT rev 6659 overlaid. The SeaWinds data swath represents about 12 minutes of data collection, centered at 2207 UTC. SeaWinds data flagged as rain-contaminated are highlighted in blue. NCEP mean sea-level pressure analysis is valid 0000 UTC.

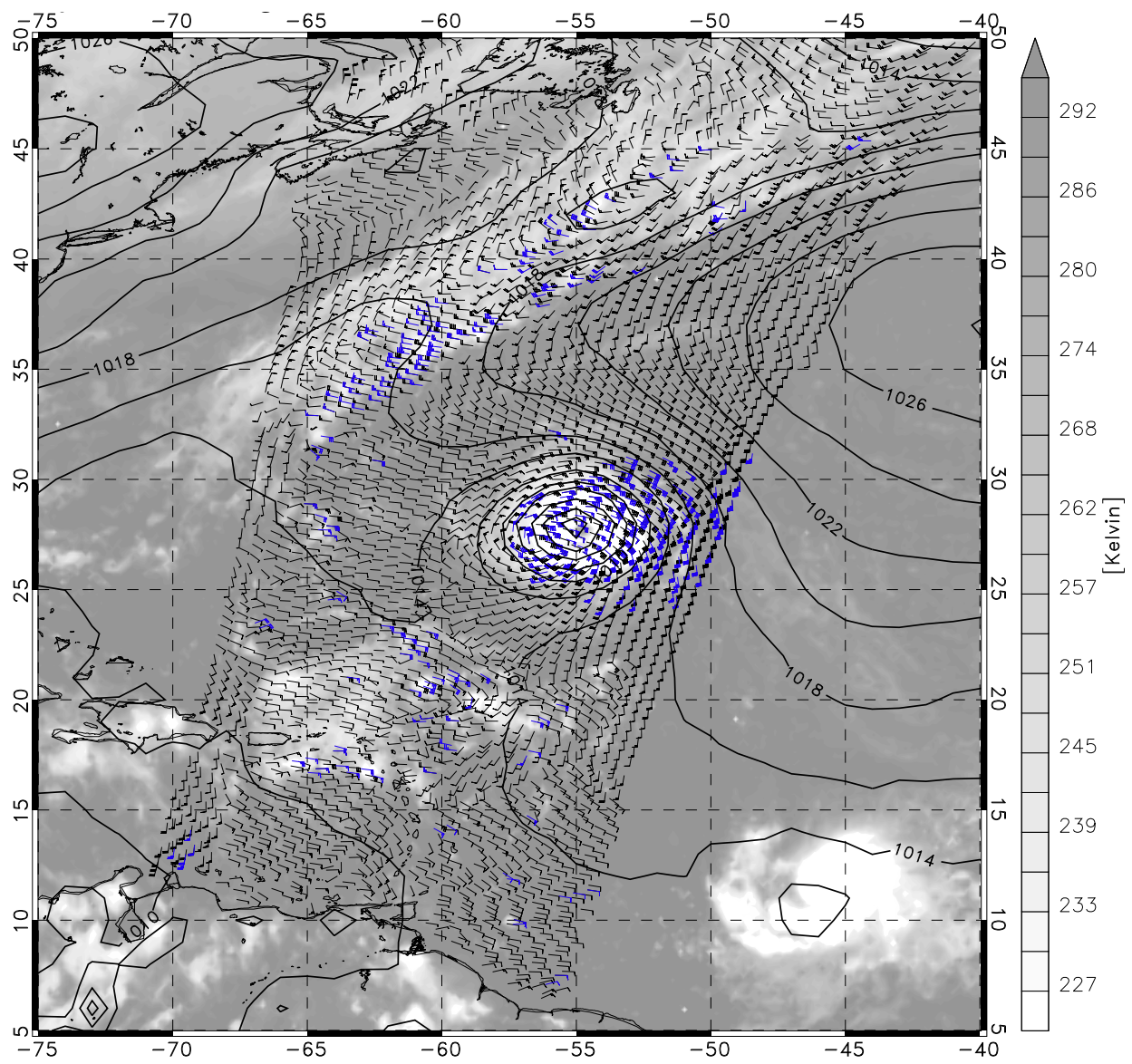


**Fig. 2:**

An example of the impact of SeaWinds data on a variational analysis. Upper left panel shows the background wind field used in 2d-VAR in the vicinity of a synoptic front. The background field is 3-hour forecast from NCEP's global model, valid at 2100 UTC 28 September 2002. Streamlines are overlaid to highlight instantaneous features in the flow. The upper right and lower left panels show 2d-VAR NORAIN and ALLOBS analyses, respectively. For verification, the lower right panel shows a GOES IR satellite image, valid 2215 UTC, and a sea-level pressure analysis from NCEP's global model, valid 0000 UTC 29 September 2002. Scatterometer winds are included for reference (winds selected by the median filter are shown), valid at ~ 2207 UTC 28 September 2002.

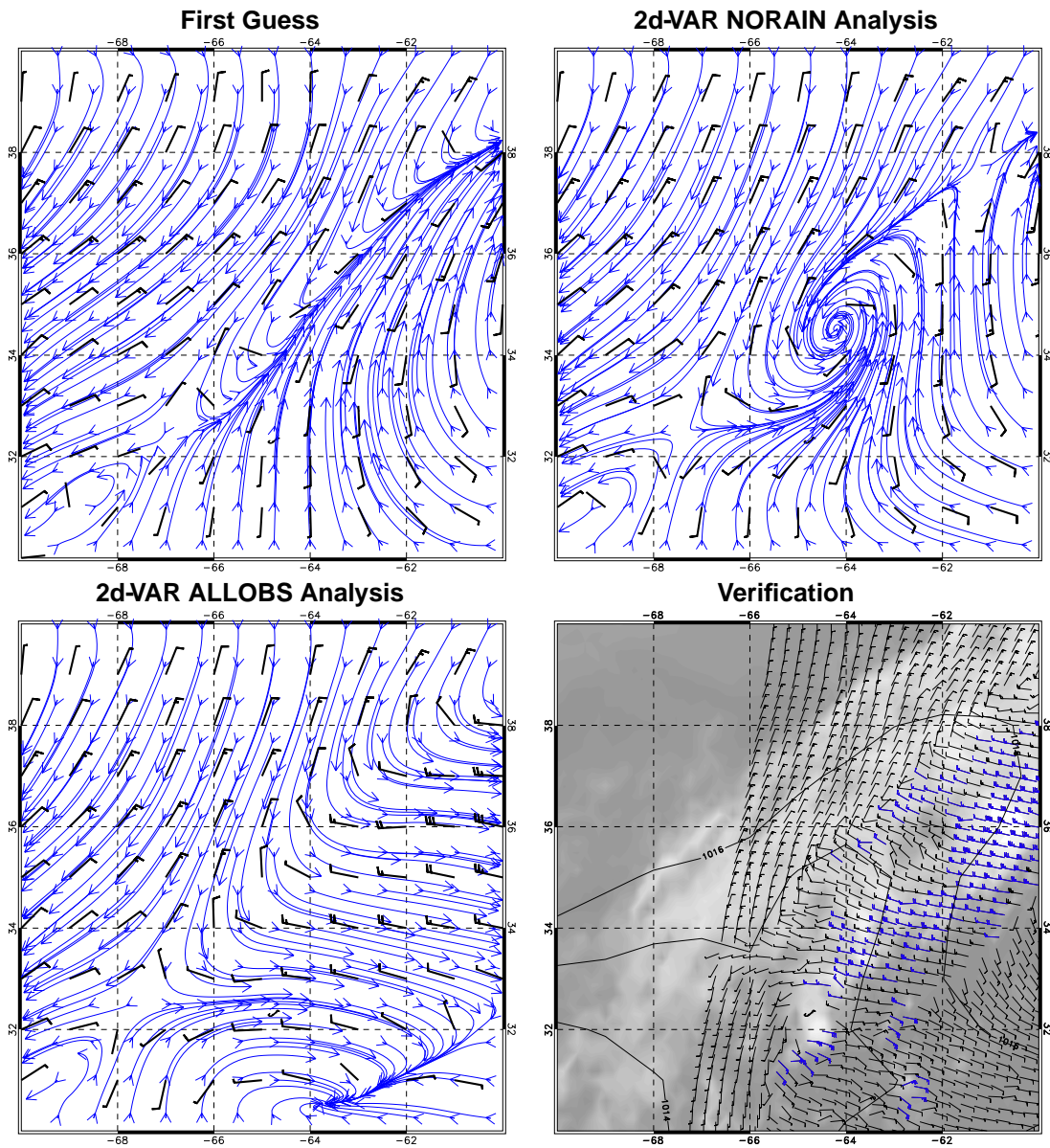


**Fig. 3:**

The QuikSCAT objective function (in dB space) plotted as a function of  $u$  and  $v$  wind components (in  $m/s$  on the abscissa and ordinate respectively). The retrieved winds are plotted as arrows. The data used are from the NRT product for rev 6937, row 542, cell 60, observed 0942 UT 18 October 2000. The top panel considers only a single backscatter measurement, the middle panel two, and the lower panel all four. The locus of  $(u, v)$  which exactly fit an individual backscatter measurement is plotted as a dotted line using the color code indicated at the bottom of panels. For reference, in the lower panel, the global minimum of the objective function is  $\sim 1.3$ . It attains a value of 73,998 at the origin in  $(u, v)$  space. For clarity, the objective functions have been shifted, truncated, and converted to dB space as described in the text.

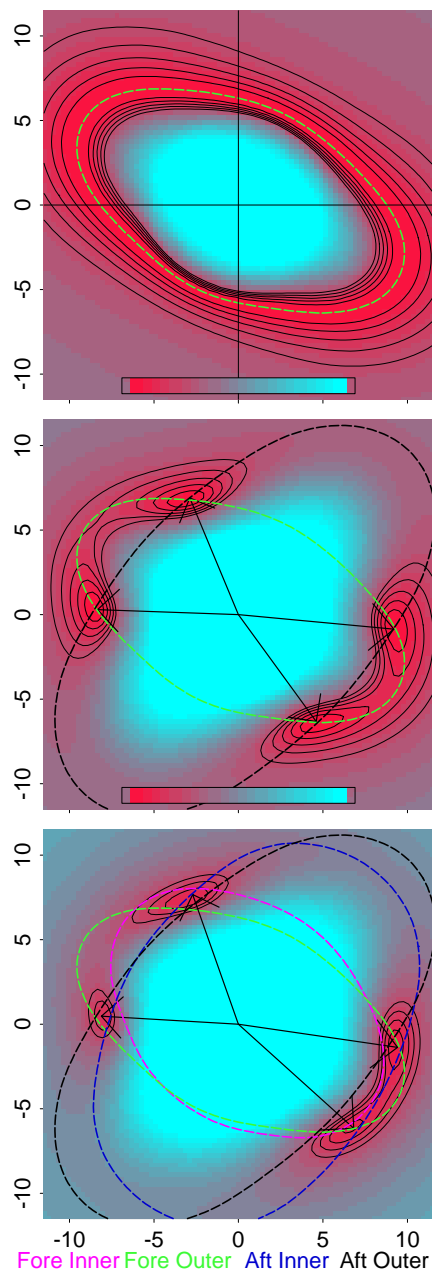
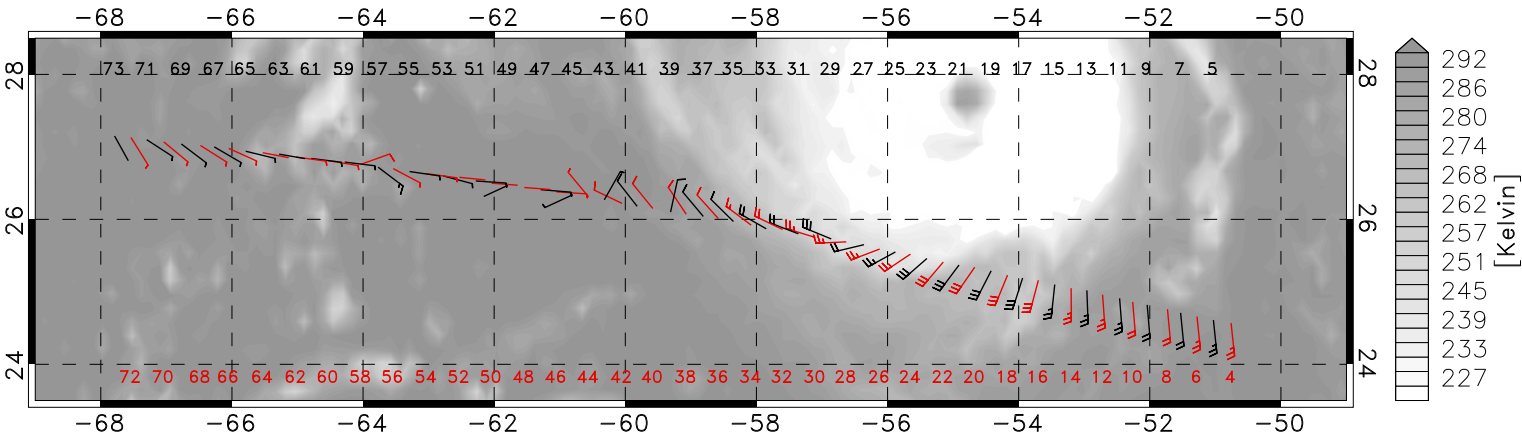


**Fig. 4:** The QuikSCAT objective function (as in the bottom panel of Fig. 3) showing different ambiguity patterns. These data are for rev 6659, row 1100, and cells 38, 18, and 4. The selected ambiguity is plotted with a wide line.



**nadir (WVC 38)**

**sweet (WVC 18)**

**far swath (WVC 4)**

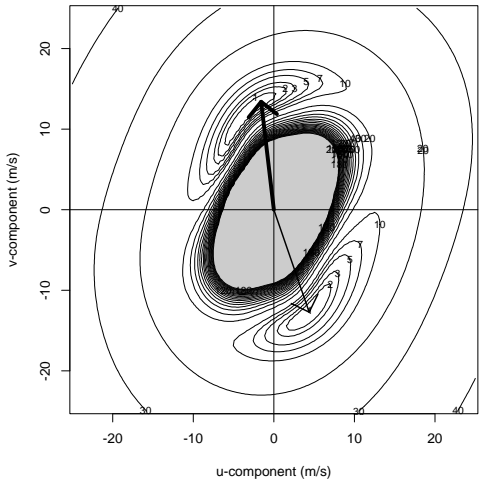
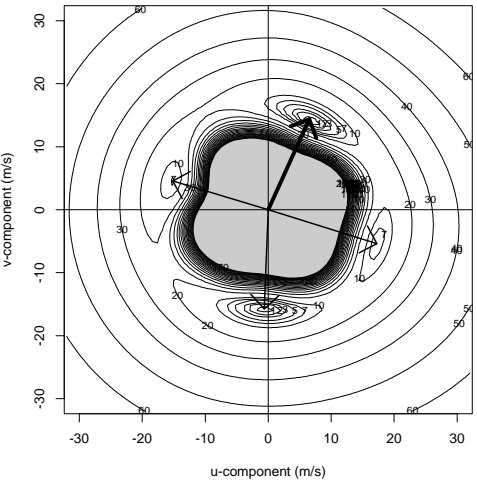
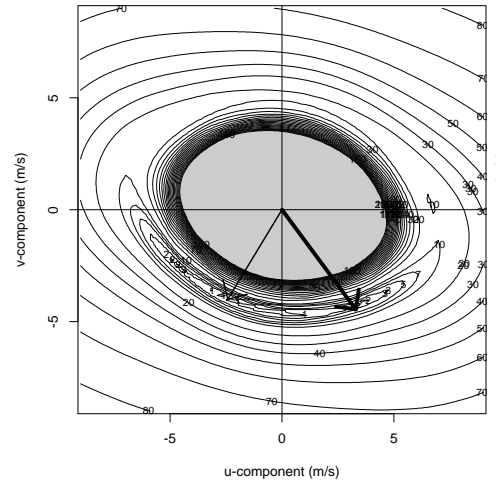


**Fig. 5:**

The QuikSCAT objective function for a very low winds case. The example is cell 48 from the wind vector cell row presented in the previous figure (Fig. 4, upper panel). The four observed  $\sigma^0$  values (ordered as they were measured by SeaWinds) are: outer-fore  $5.61107e-05$ , inner-fore:  $-3.99966e-05$ , inner-aft:  $4.15885e-05$  and outer-aft:  $-1.52102e-05$ . Notice two of the measurements are negative, an unphysical value which is an artifact of inverting the radar equation when the signal-to-noise ratio is high (see text).

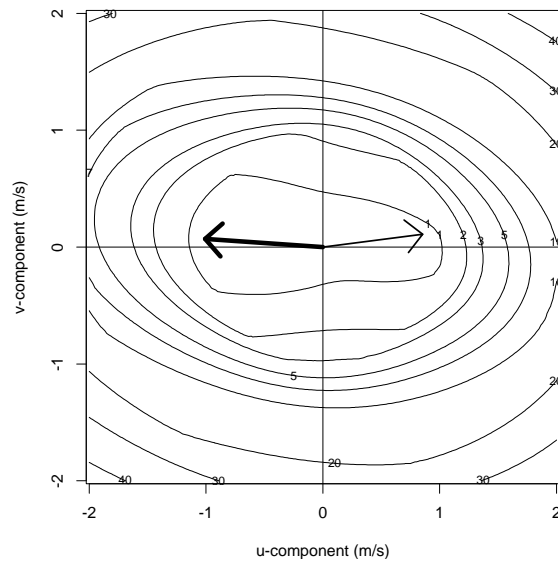


**Fig. 6:**

An example of rain-contaminated winds from SeaWinds. The upper panel shows the wind vector cell row of interest in bold wind bars. Winds suspected of rain contamination are blue. The panels below show the QuikSCAT objective wind retrieval function for cells 41, 39 and 36. Notice that the wind speeds for cell 39 are very large compared to its neighbors, and the minima in the objective function are much larger than in adjacent, non-raining cells.

